Part 8

4D-VAR assimilation of FASTEX radiosonde and dropsonde data in IOP 17: towards a reference analysis of FASTEX data

by

Gerald Desroziers*, Béatrice Pouponneau*, Jean-Noel Thépaut*, Marta Janisková** and Fabrice Veersé*.

**Météo-France, URA CNRS 1357, Groupe d'Etude de l'Atmosphère Météorologique, Toulouse, France,*

***Slovak HydroMeteorological Institute, Bratislava, Slovakia.*

8.1 Introduction

One of the main objectives of the FASTEX experiment was to improve the description of the complete life-cycle of a number of cyclones in the Northern Atlantic ocean (Joly et al., 1997). This observation set especially included a large number of additional vertical profiles performed by land-based sounding sites or ships, but also provided by dropsondes launched by aircraft. Some of the dropsonde legs designed to sample some particular features of a developing or mature cyclone can be vertically and horizontally interpolated in a vertical cross-section. Such an approach has for example already been applied by Thorpe and Clough (1991), or Browning et al. (1995) in order to present the mesoscale structures of a number of cyclones observed during FRONTS 87 and FRONTS 92 experiments. Other authors, like Shapiro and Hastings (1973) or Keyser and Shapiro (1986) also used temporal vertical cross-sections , with profiles performed at a single site, in order to recover lower and upper structures associated with fronts.

Figure 8.1: *Dates and times of the soundings performed during IOP 17, between 09 UTC 17 February and 03 UTC 20 February, by the FASTEX land-based sites, the four FASTEX ships, the two ASAP vessels inside the FASTEX zone during this period, a NSF Lear 36 flight, three NOAA Gulfstream IV flights and a UKMO C130 flight.*

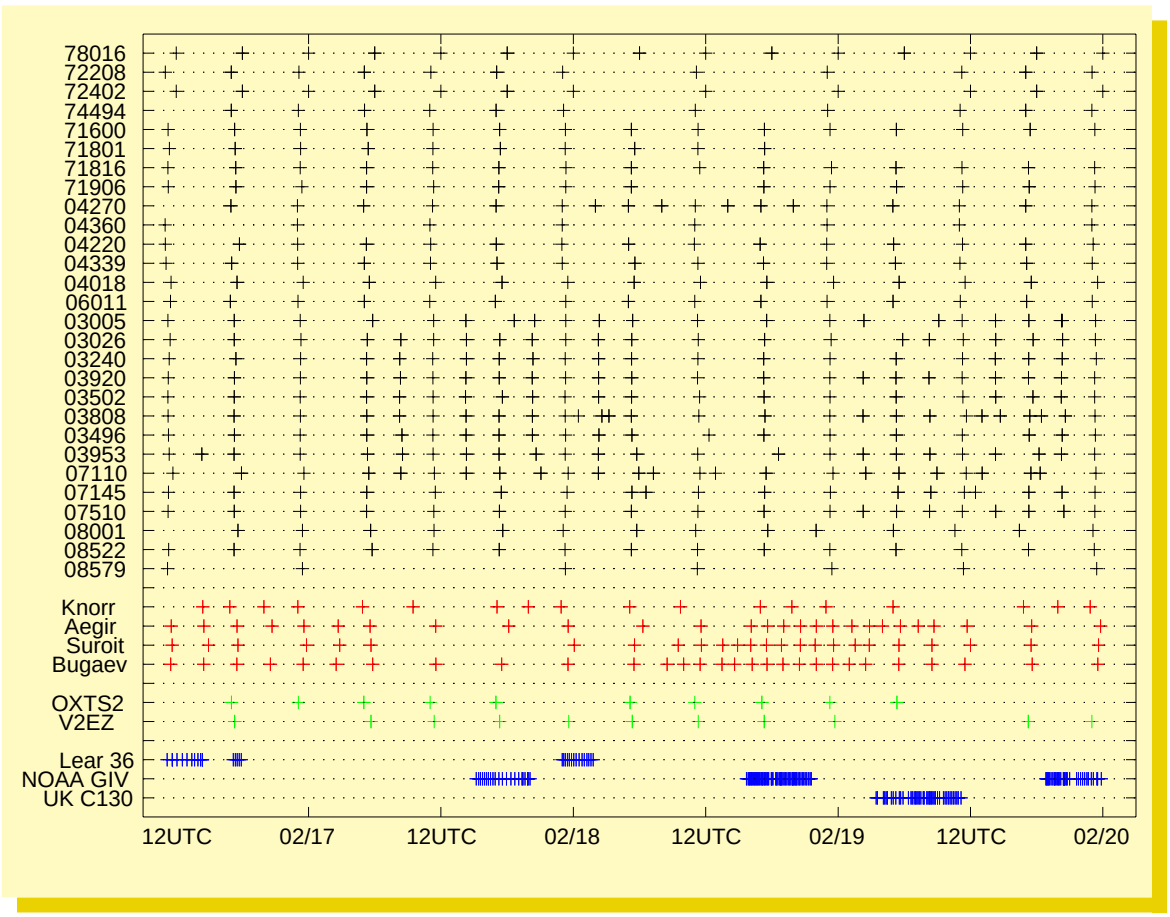

Another approach is to add such particular data collected during an experiment to the conventional dataset and to use an assimilation scheme in order to recover the complete 3-dimensional structures associated with the observed cyclones. This strategy has for example been followed by Browning et al. (1996), using the UK Meteorological Office (UKMO) assimilation scheme with FRONTS 92 dropsondes.

Our objective is to perform a complete analysis of the FASTEX cases, or at least of a number of them, since these 3D composite views of the observed systems are required for diagnostic studies, model initialization but also for the evaluation of adaptive observations as it has been settled during FASTEX (Bergot 1999). Because attention has been paid during FASTEX to disseminate the different vertical profiles in TEMP format on the Global Telecommunications System (GTS), some national weather services were able to include them in their operational analyses in real time. This has been done for example at Météo-France, in order to improve the quality of the short range forecasts and subsequently to ease the control of the operations during the field phase of the FASTEX project. However, this first set of analyses produced by the French meteorological service and included in the Data Base according to the work programme can be improved. Indeed, a significant further step can be taken by employing a 4D-VAR formulation. This 4D-VAR analysis tool is now under development at Météo-France and its present formulation is described in Janisková et al. (1999 , hereafter called *Jan 99*).

The aim of this part of the FASTEX report is to present an application of the 4D-VAR assimilation scheme to the cyclone observed during the Intensive Observation Period 17 (IOP 17), using the whole set of FASTEX soundings collected during this IOP. In the following section, one first describes this FASTEX observation dataset and some elements on the evolution of the system. The 4D-VAR set up and the methodology followed in this study are presented in section 8.2. Subsequent analyses are presented and discussed in section 8.3 and 8.4 and final conclusions and perspectives are given in section 8.5. Further results can be found in Desroziers et al., 1999.

8.2 Experiments settings and design, choice of case

8.2.1 4D-VAR setting

Here, one focusses on the way some particular FASTEX datasets are used by this analysis scheme, rather than the technique itself, which is summarized in the Short Note 8.1. According to the tests presented in *Jan 99*, the incremental 4D-VAR setting will be here fixed to the one that gave sensible results: in all the following 4D-VAR experiments, one uses three updates of the trajectory and the reduced set of simplified physics, presented in *Jan 99*, is made active only in the last minimization of the cost function specified in this variational procedure. Up to 70 iterations are used for the whole analysis, with 25 adiabatic iterations in the first two minimizations and 20 iterations with the reduced simplified physical parametrizations in the last minimization. This parametrization set includes the computation of vertical turbulent diffusion, orographic gravity waves and stratiform precipitation but excludes radiation and deep convection. A 6-hour assimilation period is used, centred on synoptic times, with a surface analysis performed at the end of the filtered variational analysis of the upper fields.

The ARPEGE French forecast model (Courtier et al. 1991) is used to give the trajectory. This spectral model is based on a stretched geometry (Schmidt 1977;

Short Note 8.1: Some details of the 4D-VAR data assimilation

by M. Janisková, F. Veersé and J.N. Thépaut

8.1.1 The incremental 4D-VAR formulation

The standard formulation of 4D-Var (Le Dimet and Talagrand, 1986) consists in determining the model trajectory which best fits the observations over a given time period $[t_0, t_f]$ and a background field (a priori estimate) at time t_0, by minimizing the cost function:

$$\begin{aligned} &\mathcal{J}(\mathbf{x}(t_0)) \\ &= \mathcal{J}^b(\mathbf{x}(t_0)) + \mathcal{J}^o(\mathbf{x}(t_0)) \qquad \text{(SN8.1.1)} \\ &= \frac{1}{2}\left[\mathbf{x}(t_0) - \mathbf{x}^b(t_0)\right]^T \mathbf{B}^{-1}\left[\mathbf{x}(t_0) - \mathbf{x}^b(t_0)\right] \\ &\quad + \frac{1}{2}\sum_{i=0}^{n}\left[H_i\mathbf{x}(t_i) - \mathbf{y}_i^o\right]^T \mathbf{R}_i^{-1}\left[H_i\mathbf{x}(t_i) - \mathbf{y}_i^o\right] \end{aligned}$$

where:

- $\mathbf{x}(t_0)$ is the initial state of the model;
- $\mathcal{J}^b(\mathbf{x}(t_0))$ is the background cost function, that is the distance at the initial time t_0 of the model state to the background field $\mathbf{x}^b(t_0)$. The latter, which usually results from a forecast valid at the initial time t_0, is an a priori estimate of the optimal initial condition and essentially summarizes the past information of the atmosphere;
- $\mathbf{B}$ is the covariance matrix of background error;
- $\mathcal{J}^o(\mathbf{x}(t_0))$ is the distance of the model to the observations over the time period;
- $\mathbf{y}_i^o$ is the observation vector at time t_i;
- H_i is the observation operator at time t_i. It allows the computation of the model-equivalent observations from the model state $\mathbf{x}(t_i)$ at this time;
- $\mathbf{x}(t_i) = M(t_i, t_0)\mathbf{x}(t_0)$ is the model state at time t_i;
- $\mathbf{R}_i$ is the observation error covariance matrix at time t_i, which accounts for measurement and representativeness errors.

In the incremental formulation (Courtier *et al.*, 1994; Ide *et al.*, 1997; Laroche and Gauthier, 1998; Veersé and Thépaut, 1998) the model and the observation operators H_i are linearized and a "simplified" correction $\delta\mathbf{w}(t_0)$ to the initial condition is determined, instead of the full system SN8.1.1, by minimizing the following quadratic cost function:

$$\begin{aligned} &\mathcal{J}(\delta\mathbf{w}(t_0)) \\ &= \frac{1}{2}\left[\delta\mathbf{w}(t_0) + \mathbf{w}^g(t_0) - \mathbf{w}^b(t_0)\right]^T \mathbf{B}_{(w)}^{-1} \\ &\quad \left[\delta\mathbf{w}(t_0) + \mathbf{w}^g(t_0) - \mathbf{w}^b(t_0)\right] \qquad \text{(SN8.1.2)} \\ &\quad + \frac{1}{2}\sum_{i=0}^{n}\left[\mathbf{G}_i\delta\mathbf{w}(t_i) - \mathbf{d}_i\right]^T \mathbf{R}_i^{-1}\left[\mathbf{G}_i\delta\mathbf{w}(t_i) - \mathbf{d}_i\right] \end{aligned}$$

where

- $\mathbf{d}_i = \mathbf{y}_i^o - H_i\mathbf{x}^g(t_i)$ are the innovation vectors, $\mathbf{x}^g(t_i)$ being the model state at time t_i issued from the first-guess field $\mathbf{x}^g(t_0)$ (initially equal to the background field $\mathbf{x}^b(t_0)$);
- $\mathbf{w}^g(t_0) = S\mathbf{x}^g(t_0)$ and $\mathbf{w}^b(t_0) = S\mathbf{x}^b(t_0)$ are the simplified first-guess and background field respectively;
- S is the (possibly nonlinear) simplification operator;
- $\mathbf{B}_{(w)}^{-1}$ is the inverse of the background error covariance matrix in the simplified space;
- $\mathbf{G}_i$ is the simplified linearized observation operator;
- $\delta\mathbf{w}(t_i) = \mathbf{L}(t_i, t_0)\delta\mathbf{w}(t_0)$ is the simplified increment at time t_i, $\mathbf{L}$ being the simplified tangent linear model.

The first-guess field $\mathbf{x}^g(t_0)$ is then updated:

$$\mathbf{x}^{gnew}(t_0) = \mathbf{x}^{gold}(t_0) + (\mathbf{S}')^{-I}\delta\mathbf{w}(t_0) \qquad \text{(SN8.1.3)}$$

where $(\mathbf{S}')^{-I}$ is the generalized inverse of the linearized simplification operator.
The whole process (minimization of the quadratic incremental cost function and updating of the first-guess) is then repeated a number of times to account for the nonlinearities in the model and in the observation operators (this is the so-called "outer loop" of the incremental 4D-Var process).

8.1.2 Description of the system

The operational model at Météo-France is part of the ARPEGE/IFS system developed jointly with ECMWF. It is a global spectral model with a terrain-following pressure-based hybrid vertical coordinate η (Simmons and Burridge, 1981). On the horizontal the prognostic variables and the orography are discretized using triangular truncated series of spherical harmonics.

A specificity of the ARPEGE model is the use of a conformal transformation of the η surfaces to obtain an increased resolution on a geographical zone of interest (Courtier and Geleyn, 1988; Hardiker, 1997). Such an irregular (hereafter denoted *stretched*) grid leads to some difficulties regarding the specification of the background error covariances (Desroziers *et al.*, 1995) and may require an adequate modeling of representativeness errors (Desroziers *et al.*, 1997). As a first step it has been decided to compute the analysis increments on a regular *unstretched* grid in the present incremental 4D-Var data assimilation system. The innovation vectors $\mathbf{d}_i$ are computed using a model at triangular truncation T95, with 27 hybrid vertical levels and a stretching coefficient equal to 3.5 (as defined in Courtier and Geleyn, 1988). The minimizations of the quadratic incremental cost functions are performed at truncation T63, with the same vertical levels but on a reduced unstretched Gaussian grid (Naughton *et al.*, 1996). This configuration is denoted in short by T95L27C3.5/T63L27C1.0. An option is included in the system for initializing the updated first-guess fields using an incremental digital filter (Lynch *et al.*, 1997).

As stated in the introduction, the incremental approach allows for an improvement of the simplified tangent linear model $\mathbf{L}$ by introducing some physical parametrizations progressively. A complete set of simplified physical parametrizations has been developed (Janisková *et al.*, 1998) including a simplified computation of radiation, vertical turbulent diffusion, orographic gravity waves, deep convection and stratiform precipitation fluxes. The simplifications aim at having the parametrization schemes as much differentiable as possible, while remaining as close as possible to the full physical parametrizations of the complete forecast model. This approach should ensure a correct direction of the physical tendencies even if the intensities of the physical processes are different. This is supposed to be sufficient for transporting adequately the perturbation $\delta\mathbf{w}$ in time.

After some trials the following configuration was established for the experiments reported in this part, with three passes in the outer loop. 25 iterations of the limited-memory quasi-Newton algorithm are used in the first two minimizations, using the simplified adiabatic model. Then 20 iterations are used for the last minimization with either the adiabatic, or simplified physics models. As stated above, the digital filters are used only after the last update, to initialize the final upper-air variational analysed fields. The background term $\mathcal{J}^b$ used in the 4D-Var experiments is identical to the one used in the French operational 3D-Var scheme (Thépaut *et al.*, 1998). It is based on a generalized linear balance operator. The specified structure functions are multivariate, non separable and latitude dependent (Bouttier *et al.*, 1997), as used in the operational suite. The minimization itself is performed using a limited-memory quasi-Newton code from INRIA (Gilbert and Lemaréchal, 1989).

Courtier and Geleyn 1988). In these experiments, the model is used with a T95 spectral truncation on the stretched sphere and a stretching factor 3.5, that provides a roughly $L = 180$ km resolution near Newfoundland and a $L = 70$ km resolution near Ireland, using the $L = (4\pi)^{1/2}a/(N+1)$ formula proposed by Laprise (1992), where N stands for the spectral resolution and a for the earth radius.

On the other part, the successive minimizations, around the different trajectories with this stretched model, are performed using a non-stretched tangent linear model and its adjoint with a $N = 63$ spectral truncation, corresponding to an uniform $L = 370$ km resolution using the previous formula again. In the vertical, both the model for the trajectory and the tangent linear model for the inner minimizations are used with the same 27 η-levels.

8.2.2 Choice of case

One focusses on the system associated with IOP 17, which occurred between 17 February and 20 February and has shown one of the strongest deepening rate observed in FASTEX. It has also been one of the best documented case of the experiment, indeed, of the history of meteorology to date. A quick-look summary of IOP 17 is shown in section 3.21 of Part 3, page 118 of this Report.

A detailed synoptic-dynamic overview of IOP 17 is proposed by Cammas et al. (1999). Using a manipulation of initial conditions through potential vorticity, Arbo-

Figure 8.2: *(a) background field, wind speed at 18 UTC 18 February and at 250 hPa (contours in solid lines every 5 m/s and only for values above 50 m/s), superimposed on potential vorticity on the 310 K isentropic surface (contours in dashed lines every 1 PV unit and for values more than 1 PV unit; values between 1 and 3 PV units are shaded); (b) 4D-VAR analysis using only the soundings given by the FASTEX ships (circles with the symbol × inside) and ASAP ships (circles with the symbol + inside); (c) 4D-VAR analysis using only the conventional data; (d) 4D-VAR analysis using both conventional data and FASTEX ship soundings; (e) 3D-VAR analysis using only the soundings closest to the synoptic analysis time; (f) 4D-VAR analysis using the same observations as (e).*

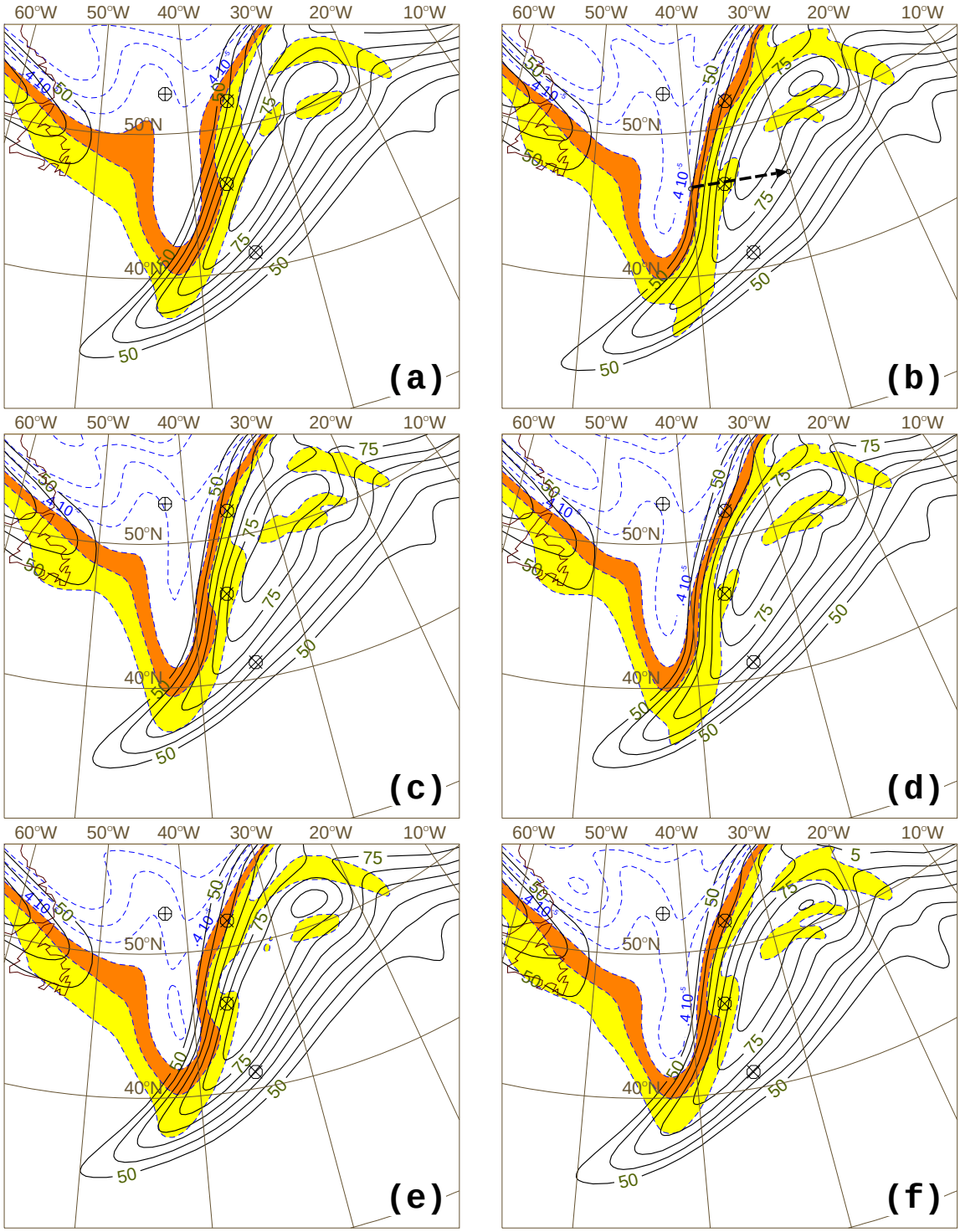

gast and Joly (1998) have also shown in a direct way the triggering features in the initial conditions.

Here, the goal is to exploit fully the available profiles and turn them into a set of reference fields. The present study concentrates on the mature stage of the system and investigate the ability of the FASTEX observing network and of the assimilation scheme to recover some realistic structures of the developed cyclone, and in particular the organization of the humidity field, directly related to the cloud system.

Figure 8.1 indicates the set of soundings performed during IOP 17, by land-based upper-air stations, FASTEX ships, ASAP ships and aircraft having launched dropsondes. Land-based upper-air stations all around the North-Atlantic basin performed soundings at 06 UTC and 18 UTC and a number of UK, French, and Irish stations also made soundings at 03 UTC, 09 UTC, 15 UTC and 21 UTC, from 00 UTC 19 February until 00 UTC 20 February, during the mature stage of the system. From figure 8.1, it also appears that three of the FASTEX ships, namely the Ægir, Suroit and Victor Bugaev, performed up to 1.5-hourly radio-soundings from 09 UTC 18 February to 12 UTC 19 February. The fourth FASTEX ship, the US research vessel Knorr, was taking part during this period to a parallel experiment in the Labrador Sea.

On 18 February, it appears that the three FASTEX ships were quite well located with respect to the developing low. Two ASAP ships, with WMO station Ids OXTS2 and V2EZ, also performed additional soundings at 06 UTC and 18 UTC during that period, the last ship V2EZ being also located close to the system. At that time, the cyclone has developed a cloud band associated with the cold front and a well formed cloud head above the surface low. The system has also been sampled by a NOAA Gulfstream-IV flight from St-John's to Shannon, between 1541 UTC and 2134 UTC 18 February with 54 launched dropsondes. Around 18 UTC, this aircraft jet passed just above the French Suroit vessel.

Twelve hours later, at 06 UTC 19 February, the low was even deeper and the cloud head was associated with a bent-back warm front and a dry zone entering between this back-bent front and the cold front. At that time, the UKMO C130 aircraft performed a flight, from 0327 UTC to 1109 UTC 19 February with 44 dropsondes, in order to observe the mesoscale structures within this region.

Here, most of the soundings found in the FASTEX Data Base are used. However for some flights, as the NOAA Gulfstream-IV flight, providing dropsondes with a very high horizontal density (up to 20-30 km), a data selection of these dropsondes has been performed, since some preliminary tests with FRONTS 92 dropsondes (Browning et al., 1995) and an incremental 3D-VAR scheme showed that a problem of representativeness error could occur with a too coarse analysis increment (Desroziers et al., 1997).

All the FASTEX vertical profiles are also available in the central archive with a very high vertical resolution. However for the time being, only the TEMP format versions of these profiles have been used, due to the largely coarser vertical resolution of the analysis compared to the high resolution FASTEX soundings. An intermediate way to handle these high resolution profiles would be to compute averaged profiles that could be better compared to their model equivalents in the vertical.

Among the advantages of using 4D-VAR, one of them is to enable the use of the observations at their true dates and times. This is particularly important, since it allows the use of all the vertical profiles performed with a high cadence by the FASTEX ships but also dropsondes given by long duration flights, with launching time departures up to 3 hours.

Figure 8.3: *(a) background field, θ_w at 18 UTC 18 February and at 950 hPa (shaded contours every 1°C and only from 280°K to 284°K) superimposed to the vertical velocity at 600 hPa (contours in thin lines every 2 Pa/s, upward velocity dashed), and to mean sea level pressure (contours every 5 hPa in thick solid lines); (b) 4D-VAR analysis of the same fields as (a), the only observations being the soundings from the FASTEX ships (circles with the symbol × inside) and ASAP ships (circles with the symbol + inside).*

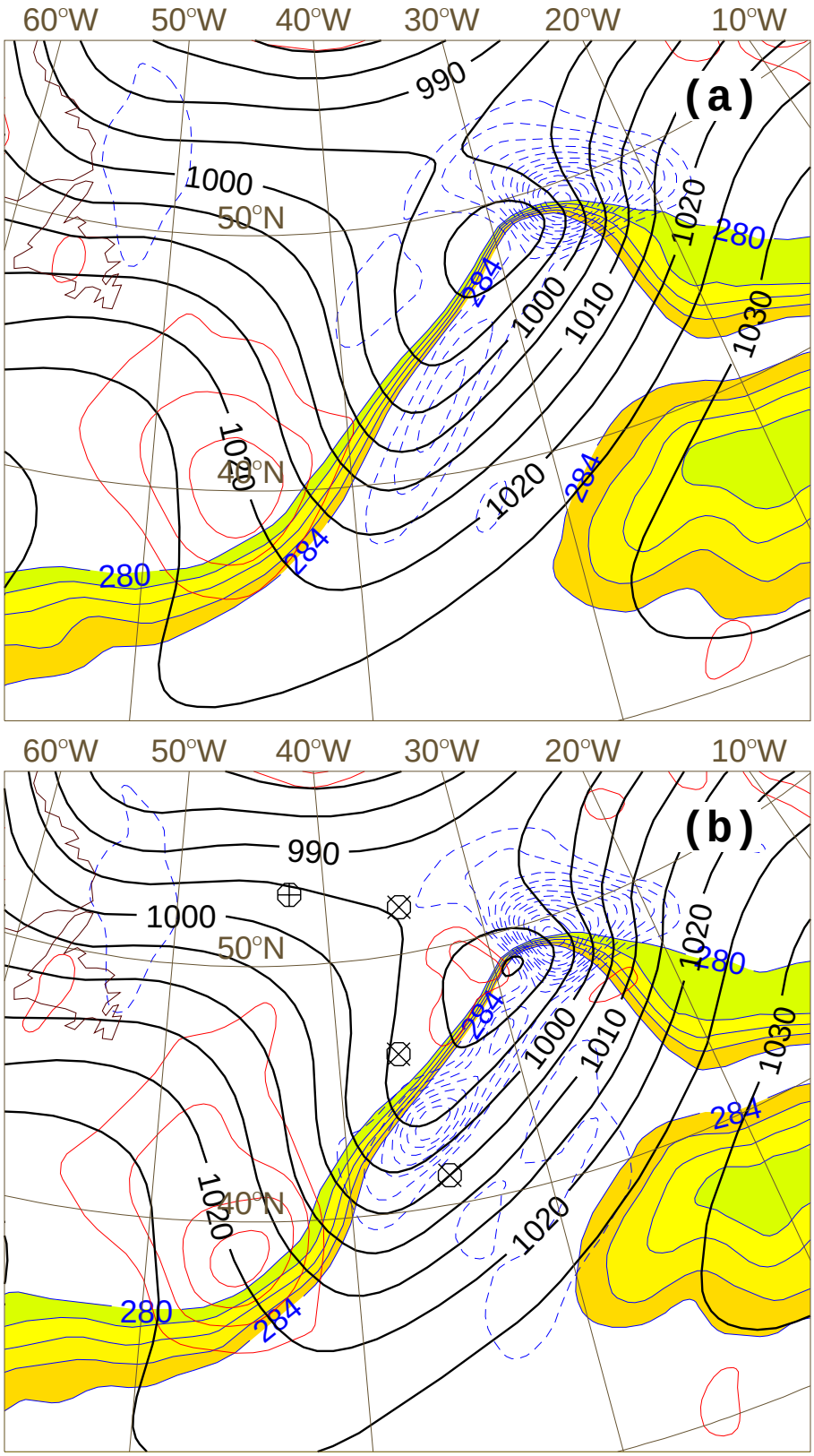

8.3 Analyses at 18 UTC 18 February 1997

In this section, one investigates the impact of the FASTEX data on the final analyses, but also the role of the assimilation scheme used to produce these analyses. In order to document these points, different analyses are presented at 18 UTC 18 February, at the time when FASTEX ships started their intensive soundings (Fig. 8.1) and corresponding also to the mid-flight time of the St John' s–Shannon NOAA Gulfstream-IV flight. All these analyses are performed with the same background (or first guess) field, the one provided by a preliminary incremental 3D-VAR assimilation using the operational observation files as in *Jan 99*.

Figure 8.2.a presents the structure of the jet at 250 hPa, as given by this background at 18 UTC 18 February. At this time, the jet stream had split in two jet streaks (Cammas et al., 1999): the outflow jet (not shown in Fig. 8.2) and another one, which will be referred to as the polar jet, with an entrance region near 40°N - 40°W and a maximum value of about 80 m/s. Three of the FASTEX vessels were then located along the 35°W meridian (from north to south, one founds the Ægir, Suroit and Victor Bugaev vessels) and the German ASAP V2EZ was also located close to the cyclonic side of the jet.

A 4D-VAR analysis using only the soundings associated with these ships has been performed (the soundings from the FASTEX vessel Knorr and the Danish ASAP OXTS2 have also been included, but at that time their positions were far from this area of interest). We can observe that the resulting analysis for the wind velocity (Fig. 8.2.b) is different from the background one: the jet streak structure of this polar jet is reinforced, with the maximum values around 80 m/s pushed north-eastward. Also, this part of the jet now presents a more curved shape on its cyclonic side. The main point to be noted is that this characteristic curved flow appears to better fit the cyclonic curvature of the sharp edge of high altitude clouds found along the jet axis.

A 4D-VAR analysis, still based on the same background, has also been produced but using only the conventional data and excluding the previous FASTEX ship soundings. Figure 8.2.c shows that the increase of cyclonic curvature of the polar jet brought by the FASTEX ships is also suggested when using only these conventional data. Finally, a 4D-VAR analysis with both sets of data gives a representation of the jet very close to the one obtained with only the FASTEX ships (Fig. 8.2.d).

Figure 8.2 also shows the structure of the potential vorticity field on the 310 K isentropic surface. According to what has been observed on the wind field, the analysis using only the FASTEX ship soundings (Fig. 8.2.b) appears to be more different from the background representation (Fig.8.2.a) than the analysis using the conventional observations (Fig. 8.2.c): the amplitude of the potential vorticity anomaly on the south-west part of the polar jet streak is increased; this is consistent with the above-mentioned change of the jet structure in the south-west entrance region (near 41N-41W).

In order to evaluate the impact of the intensive soundings performed by the FASTEX ships during this 6-hour assimilation period, a 3D-VAR analysis has been produced at 18 UTC, using only the FASTEX soundings closest to this synoptic time. The retrieved wind and potential vorticity analyses (Fig. 8.2.e) show far less differences with the background representations than the previous analyses obtained with 4D-VAR and all the profiles available in the 6-hour period. However, a 4D-VAR analysis including only the same subset of FASTEX ship soundings (Fig.8.2.f) appears to be closer to the one obtained with all the profiles: the maximum values of the polar jet streak are moved north-eastward and the characteristic curvature of the jet entrance

Figure 8.4: *(a) vertical and temporal cross-section of the meridional component of the wind (contours every 5 m/s), at the Suroit vessel location (46.1N-36.6W) and between 15 UTC and 21 UTC 18 February; the time has been reversed and the data have been interpolated by a spline algorithm; (b) same as (a) but for the background equivalent; (c) same as (a) and (b) but for the 4D-Var analysis with only the FASTEX ship soundings; (d), (e) and (f) respectively same as (a), (b) and (c) but for relative humidity (contours every 10 % RH).*

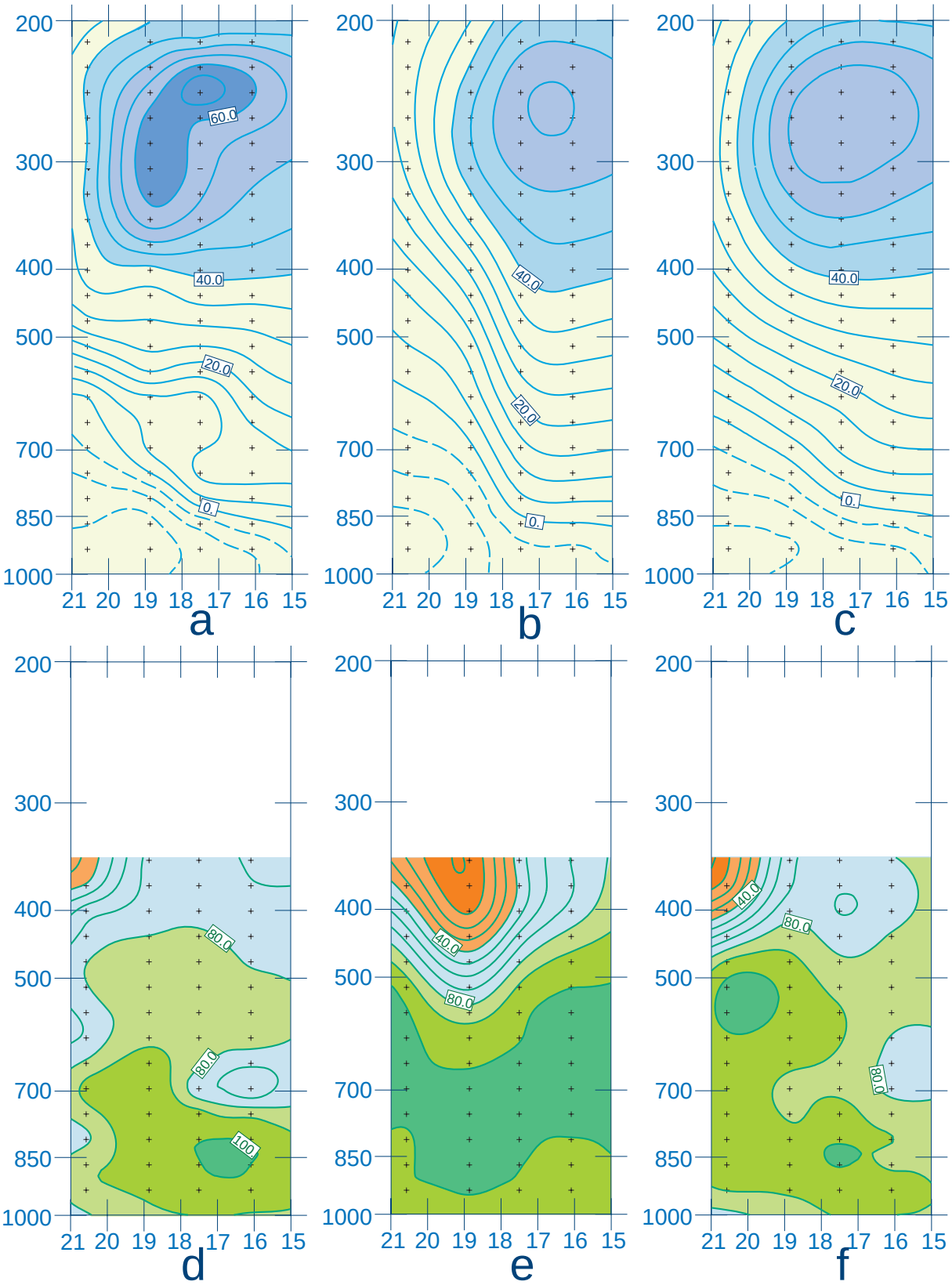

is suggested with a reinforcement of the potential vorticity anomaly. This indicates a clear improvement of 4D-VAR over 3D-VAR for this case, that can be likely related to the use of implicit dynamical structure functions by the 4D-VAR formulation, as isotropic and less realistic structure functions are used in the 3D-VAR formulation (Thépaut et al. 1996).

From a dynamical point of view, the increase of the jet curvature found near 42°N-42°W in the 4D-VAR analyses (Figs.8.2.b and d, particularly) should be associated with a dipole of mid-tropospheric descent and ascent, due to ageostrophic motions along the jet flow, with confluence and diffluence areas, respectively located upstream and downstream of this flow inflection (Keyser and Shapiro 1986). The descending vertical velocities, associated with this secondary circulation, should also reinforce the downward branch of the direct transverse ageostrophic circulation at the entrance of the jet streak axis (43°N-38°W/52°N-22°W).

The differences at low levels between the background field (Fig.8.3.a) and the 4D-VAR analysis using only the FASTEX ship soundings (Fig.8.3.b) seem to be consistent with the above-mentioned dynamical processes. These differences show a displacement and a reinforcement in the analysis of the downward velocities at 600 hPa, south-west of the PV anomaly axis (38N-45W), which is in agreement with the water-vapour image (not shown). The expected increase of upward velocities west of the latter PV anomaly axis is also found. One has to note that these likely dynamical modifications, due to ageostrophic adjustment, are a direct and positive consequence of the use of the temporal dimension in 4D-VAR.

A striking point is also the appearance of a frontal wave, quite clear in the θ_w field at 950 hPa, in the surface trough south-west of the main cyclone. This frontal wave can be observed in the measurements made by the Victor Bugaev vessel (not shown) as mentioned in Cammas *al.* (1999). The surface cyclogenesis associated with the frontal wave might be related to the reinforcement of ageostrophic vertical motions, inducing a coupling between an area of initial strong vorticity at low levels and the circulation associated with the upper PV anomaly shown in Fig. 8.2.b (Hoskins et al. 1985).

The high cadence FASTEX ship soundings performed in a meteorological active region actually makes up an unique dataset. A way to investigate how 4D-VAR handles this dataset is to look at what happens in time at a particular ship location. Figure 8.4.a shows the temporal evolution of the meridional component of the wind above the Suroit location (46.1°N-36.6°W).

The observations associated with the four soundings performed by this ship during the 6-hour assimilation period are analyzed with a spline algorithm (Desroziers and Lafore 1993). In order to filter observation and representativeness errors, a smoothing is applied, the amplitude of this smoothing being determined by an objective cross-validation method (Wahba 1980).

This figure shows that the Suroit vessel was very nicely located during this 6-hour period, since it sampled the jet structure with a characteristic sharp gradient on its cyclonic side. The background equivalent evaluations at the same time and location can also be interpolated by the previous spline algorithm, but with no additional smoothing in this case (Fig. 8.4.b). The resulting cross-section presents large differences: the maximum value of the wind is lower and the cyclonic gradient is also less important, the whole upper wind structure being too early in time in the background; the lower structure is also quite different with a too steep slope in the gradient associated with the system cold front. Figure 8.4.c presents the corresponding vertical

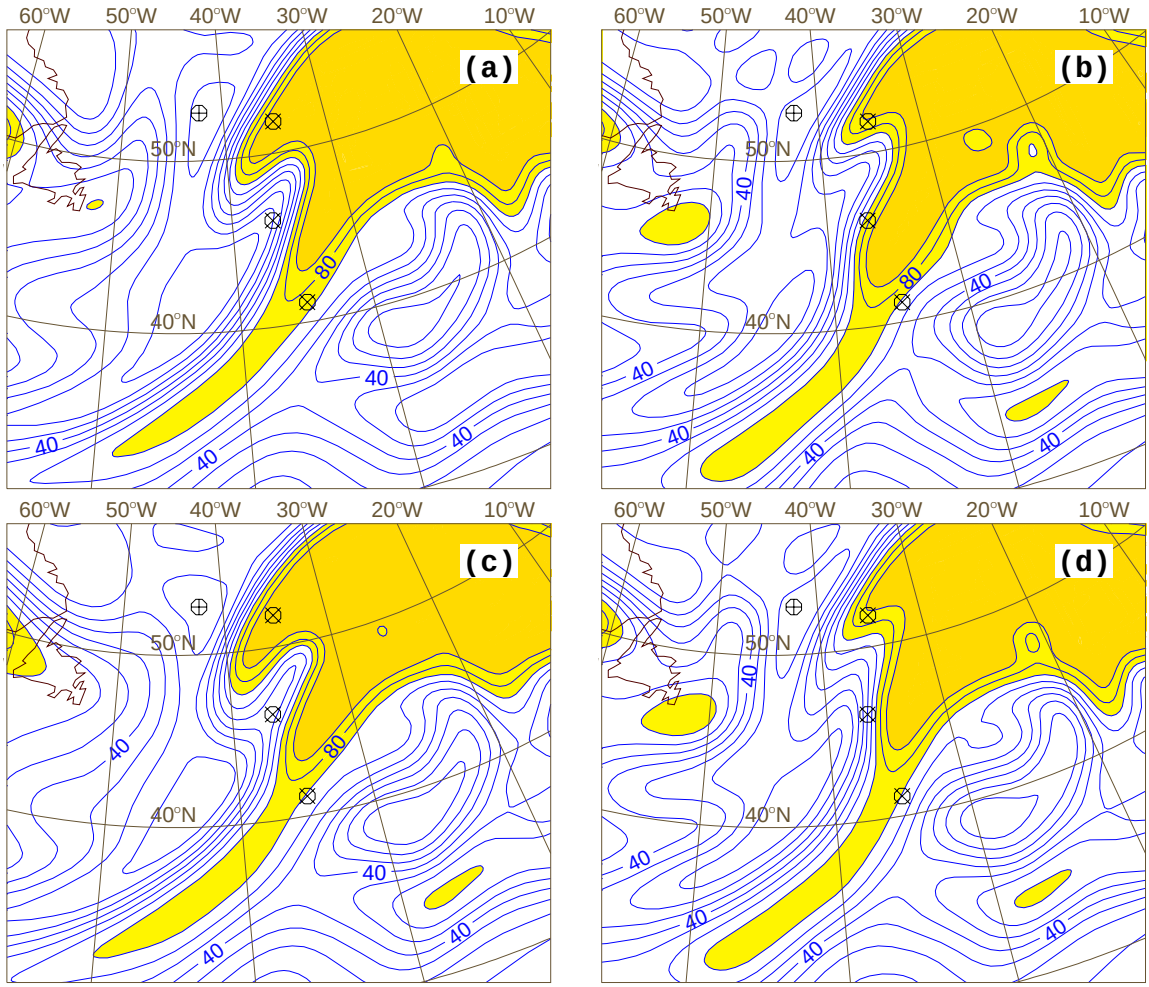

Figure 8.5: *(a) background field, relative humidity at 18 UTC 18 February and at 350 hPa (contours every 10 % RH); (b) 4D-VAR analysis using only the soundings given by the FASTEX ships (circles with the symbol × inside) and the ASAP ships (circles with the symbol + inside); (c) 3D-VAR analysis using only the soundings closest to the analysis time; (d) 4D-VAR analysis using the same restricted set of soundings as (c).*

cross-section for the 4D-VAR analysis with only the FASTEX ship soundings. This representation is much closer to the observed values: the cyclonic upper gradient of the wind is better described and the lower structure is also modified. Of course, the small details found in the observations are not retrieved but one has to keep in mind that this incremental assimilation is performed with an only T 63 tangent linear model.

The same vertical and temporal cross-sections at the Suroit location can be produced for the observation (Fig. 8.4.d), background (Fig. 8.4.e) and analysis (Fig. 8.4.f) representations of relative humidity. According to Cammas et al. (1999), the values less than 70 % RH at 400 hPa and at 21 UTC, found in Fig.8.4.d, are associated with the upper level dry air intrusion on the cyclonic side of the jet stream. The values of humidity less than 70 % RH at 700 hPa and at 16 UTC are related

to the low level part of this dry intrusion. The values more than 80 % RH below 400 hPa correspond with the above-mentioned cloud head structure associated with the system. Figure 8.4.e shows that the humidity background cross-section is quite different from the observed one: one can especially note that accordingly to the wind representation, the upper level dry air intrusion on the cyclonic side of the jet, is too early in time in the background description. This deviation between observation and background is however strikingly corrected in the final analysis (Fig. 8.4.f): the latter upper level dry air intrusion is moved backward in time and the low level dry intrusion is also suggested.

The comparison of the humidity field representations at 350 hPa, given by the different experiments (Figs. 8.5) also shows that, as for the jet description, the differences in these representations are associated with the use of a 3D or 4D-VAR analysis scheme: with the same subset of FASTEX ship soundings synchronous with synoptic time, 4D-VAR produces a description of the humidity (Fig. 8.5.d) that is much more in agreement with the vertical and temporal cross-section shown in Fig. 8.4.d, than the one obtained with 3D-VAR (Fig. 8.5.c). However, the use of the whole set of FASTEX soundings available during the 6-hour assimilation period still brings a refinement of this description (Figs. 8.5.b): the strong gradient zone in the humidity field associated with the clouds is pushed westward of the Suroit location, in agreement with the vertical cross-section found in Fig. 8.4.f. This description of the humidity field also better fits the water-vapour image.

8.4 Analysis at 06 UTC 19 February 1997

Starting from the same 3D-VAR background used to produce the previous assimilation experiments at 18 UTC 18 February, two 4D-VAR analysis cycles have been performed from 18 UTC 18 February to 06 UTC 19 February, using different datasets: a first one has been produced with the data normally available operationally with the addition of the soundings made during that period by the land-based sites around the Atlantic basin plus the profiles provided by the FASTEX and ASAP ships (experiment called A hereafter), and a second one obtained by adding the dropsondes launched by the NOAA Gulfstream-IV and the UKMO C130 during this time to the previous dataset (experiment called B hereafter).

Figures 8.6.c and d present the 4D-VAR analysis at 06 UTC 19 February resulting from the last experiment B, that is to say using all the FASTEX soundings, including the UKMO C130 dropsondes, added to the operational dataset. As mentioned above, these dropsondes were launched during a long duration and system-relative flight which makes difficult the use of the corresponding observations in an intermittent analysis scheme with an unique analysis time such as 3D-VAR: in that sense, the 4D-VAR formulation simplifies the use of such asynchronous data. The background humidity field used for this assimilation depicts the global structure of the cloud head associated with the mature cyclone (Fig. 8.6.a), with homogeneous values everywhere higher than 70 % RH. On the opposite, the retrieved analysis (Fig. 8.6.c) shows a clear tongue of dry air on the 310 K isentropic surface, just west of the UKMO C130 flight. This is in better agreement with the composite water-vapour image at 06 UTC 19 February (not shown), which shows this darker and then dryer area on the west part of the flight. This dry air intrusion, north of the main intrusion associated with the "polar jet" is likely related to the subsidence zone at the entrance of the "outflow jet" (Cammas et al. 1999). Moreover, the analyzed potential vorticity field

Figure 8.6: *(a) background field, relative humidity at 06 UTC 19 February on the 310 K isentropic surface (contours every 10 % RH) in experiment B with all FASTEX observations; (b) same as (a) but for potential vorticity (contours every .5 PV unit and between 1 and 4 PV units); the different legs of the UKMO C130 flight are also indicated and the dashed one corresponds to the cross-sections shown in Fig. 8.7; the dashed line AB indicates the location of the cross-sections presented in Fig. 8.8; (c) and (d) respectively same as (a) and (b), but for the the 4D-Var analysis B with all FASTEX observations; (e) and (f) respectively same as (a) and (b), but for the 4D-Var analysis A with all FASTEX observations but without the dropsonde data.*

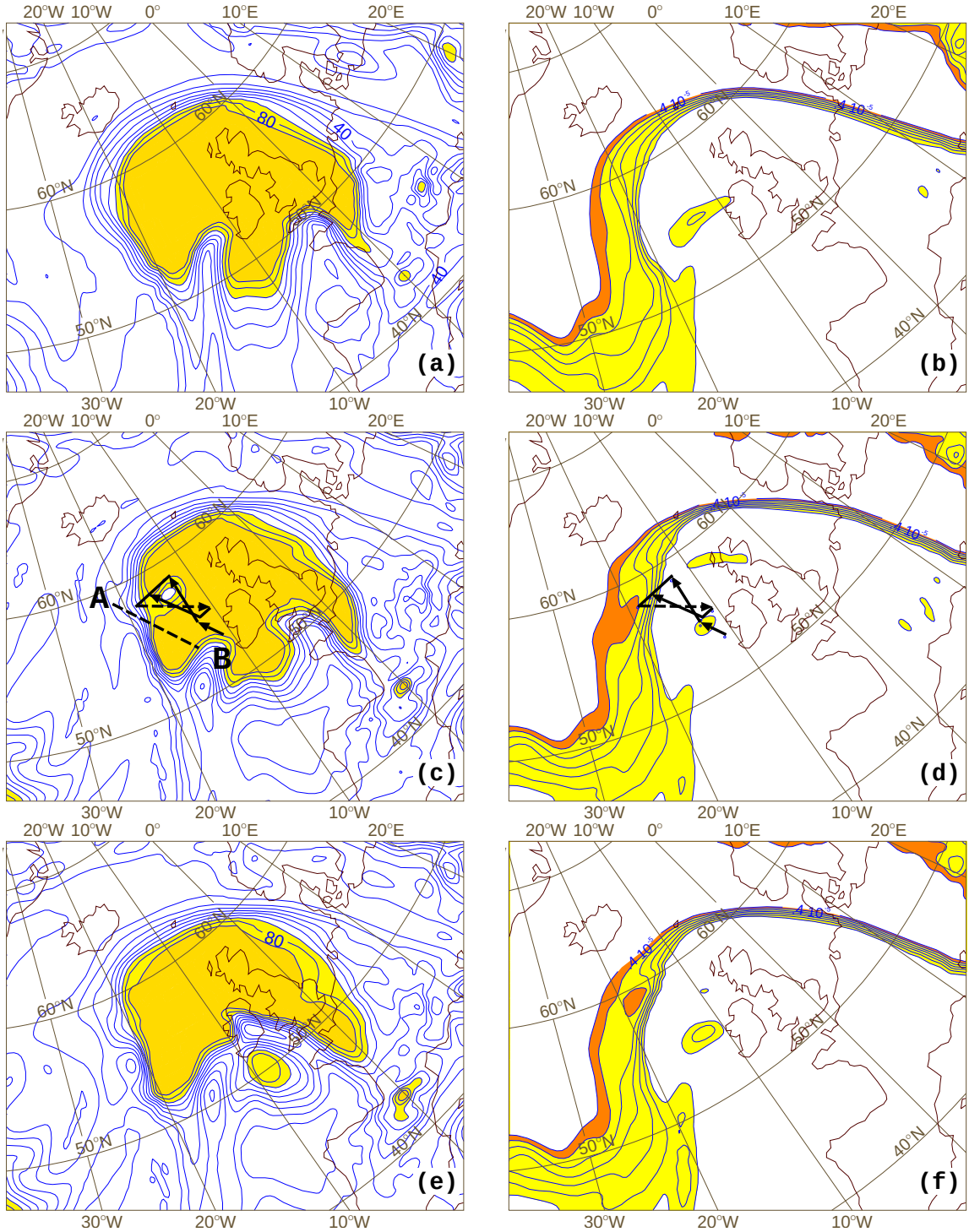

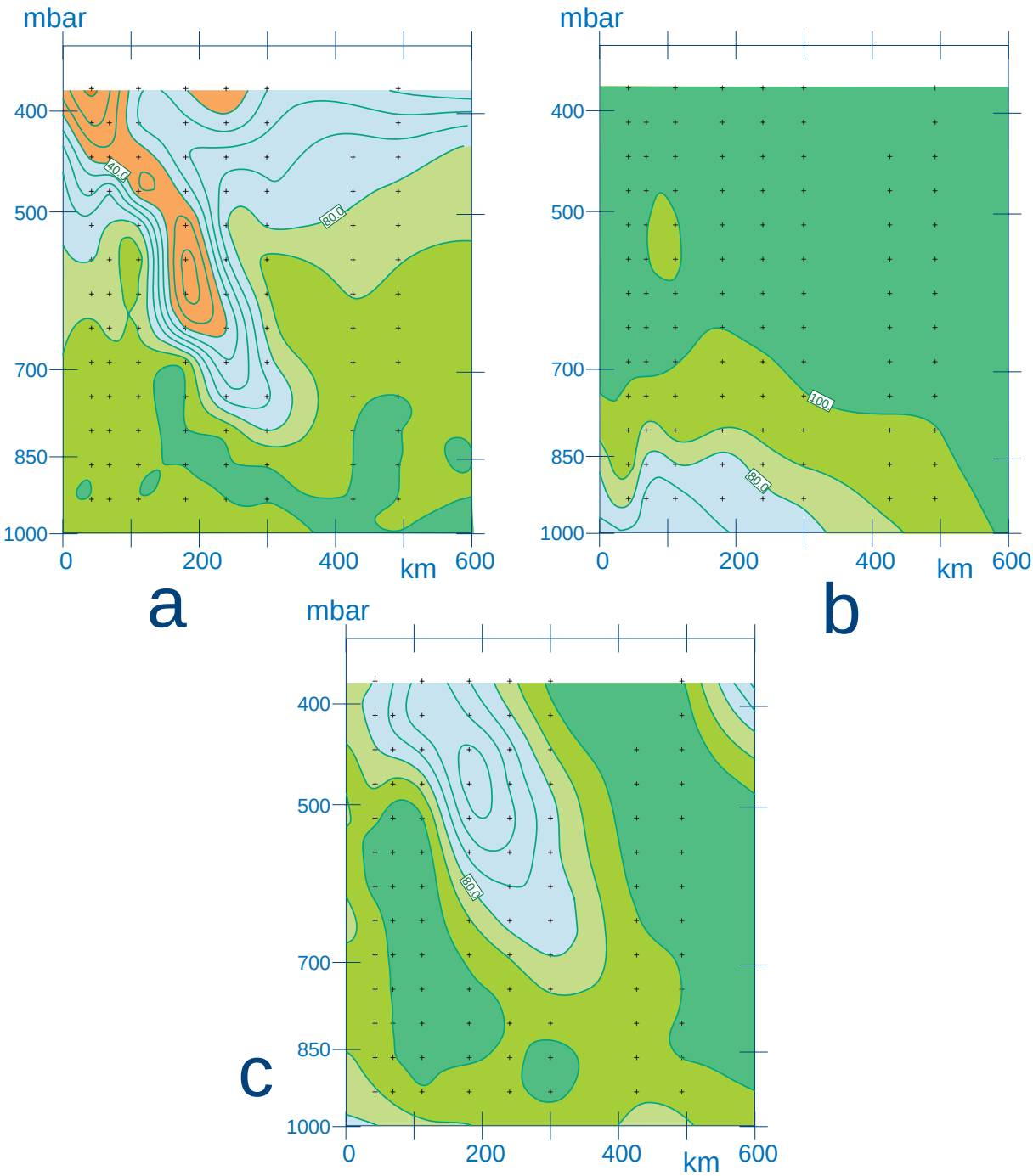

Figure 8.7: *(a) vertical cross-section of relative humidity (contours every 10 % RH) along the UKMO C130 leg defined in Fig. 8.6; (b) same as (a) but for the background field; (c) same as (a) and (b) but for the 4D-Var analysis B including all FASTEX observations.*

on the 310 K isentropic surface (Fig. 8.6.d) also presents a singularity just west of the dropsonde leg, that suggests a downward and north-eastward dry air intrusion (note that this potential anomaly is also missing in the corresponding background field found in Fig. 8.6.b). On the other hand, Figures 8.6.e and 8.6.f present the corresponding representations of the humidity and potential vorticity fields for the 4D-VAR experiment A, that is to say with no dropsonde data: they do not show the dry air intrusion, which proves that the UKMO C130 dropsondes contain an essential information not found in other observations and that this information is correctly treated by the 4D-VAR scheme.

The comparison of the observation, background and analysis descriptions along one of UKMO C130 leg (see Fig. 8.6.b for its position) confirms the correct use of the dropsonde data by the 4D-VAR analysis . In agreement with the previous horizontal views, the vertical cross-section through the background relative humidity field (Fig. 8.7.b) only presents very high values except in the lower levels. On the opposite, the vertical cross-section through the observations (Fig. 8.7.a) lets appear a narrow and tilted dry air intrusion with values everywhere less than 80 % RH. The retrieved analysis cross-section (Fig. 8.7.c) consistently depicts this dry air intrusion with in particular a good agreement in the slope of this tongue of dry air. However, the scale of this intrusion appears broader in the analysis than in the observations and the mimimum values are also larger, but one has again to keep in mind the coarse resolution of the analysis increment.

The description by the analysis of the dry intrusion structure is confirmed by the vertical cross-section presented in Fig. 8.8.a and located south-westward of the UKMO C130 flight in the dry zone appearing very clearly on the 310 K isentropic surface in Fig. 8.6.c (the position of this cross-section is also indicated in this figure). Figure 8.8.b also shows that this dry air entrance is associated with clear downward vertical velocities in this area. Moreover, these downward vertical velocities are completely absent in the background representation (Fig. 8.8.c), which proves that the whole correction to this background is dynamically consistent.

8.5 Conclusion

We have presented a case study of the use of FASTEX additional soundings in the 4D-VAR analysis formulation, including simplified and regular physical parametrizations described in the first part of this paper. The results are found to be extremelly encouraging, since this 4D-VAR analysis scheme appears to handle the FASTEX dataset consistently. The 4D-VAR formulation especially provides a natural and beneficial framework to deal with the high cadence soundings performed by the FASTEX ships: the background used in the variational procedure is modified accordingly to the observations performed by the ships. Even with the same limited dataset of observations synchronous with synoptic time, 4D-VAR provides a better analysis than 3D-VAR.

There is also a clear impact of the FASTEX observations, containing an information that is not present in the operational dataset. This is particularly evident in the case of the system-relative UKMO C130 flight which brings an essential information on fine structures of humidity and therefore of the cloud system associated with the low, but also of dynamical fields such as vertical velocity or potential vorticity.

This application of 4D-VAR to the dense FASTEX network is also considered particularly promising as these first analyses have been obtained with a low resolution

Figure 8.8: *(a) vertical cross-section along the dashed line AB in Fig. 8.6 of relative humidity in the 4D-Var analysis B including all FASTEX observations (contours every 10 % RH); (b) same as (a) but for vertical velocity w (contours every 1 Pa/s); (c) same as (b), that is w, but in the initial background field.*

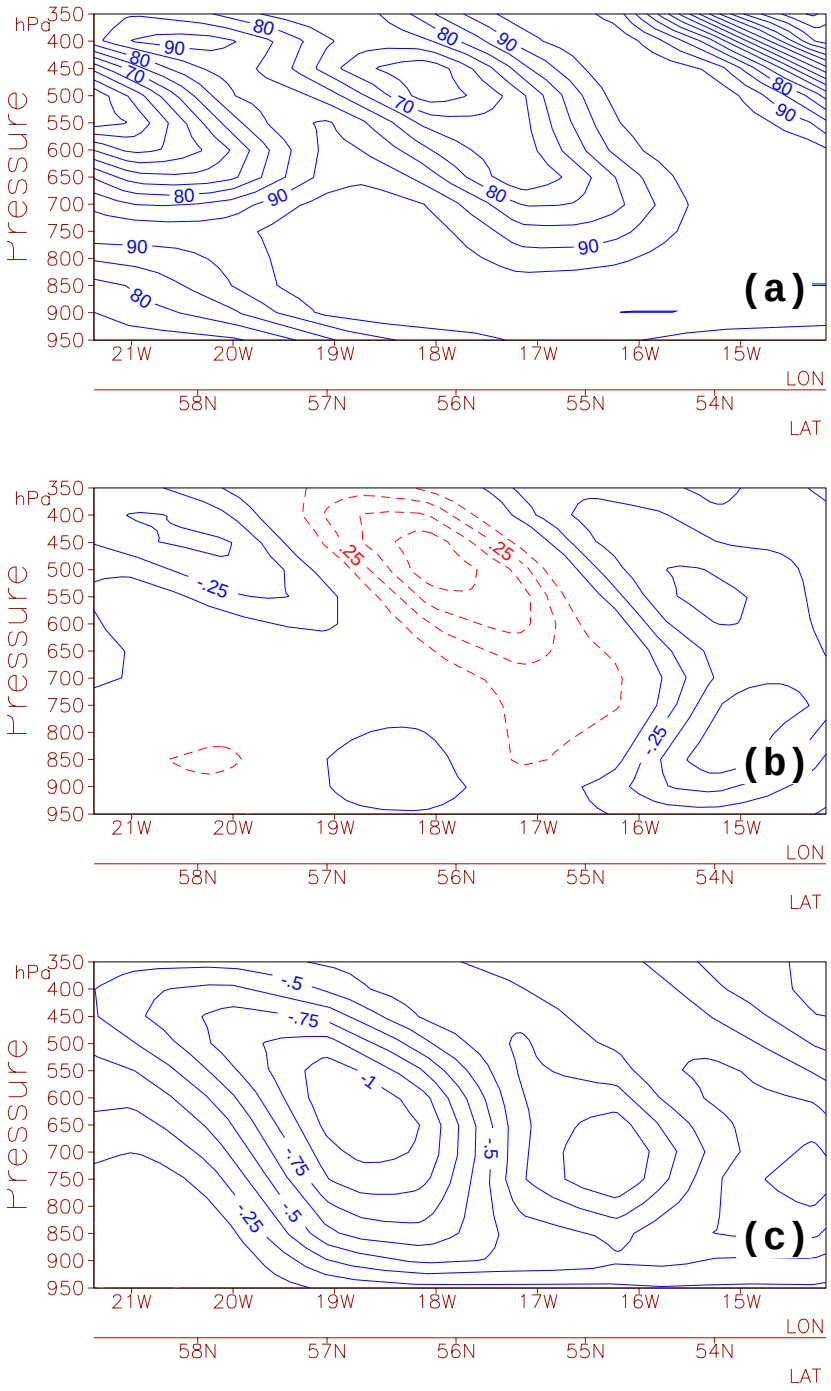

tangent linear model. However, the comparison to the high resolution FASTEX observations show that some sub-structures or strong gradient regions are mis-represented in the analysis. This suggests that there is still a scope to improve this preliminary set of analyses by increasing the resolution of the increments.

Another point of potential improvement is to increase the length of the assimilation period: according to what is known on 4D-VAR, this should still improve the way the increments between observations and background are spread in space and time.

In this part, the different analyses have been validated by looking at the proximity of the final analysis to an unused subset of FASTEX observations. This has been possible in region where these observations were dense, as in vertical cross-sections respectively sampled in time and space by ship soundings and by dropsondes. In Desroziers et al. (1999), the way the analysis came closer to a FASTEX subset of observations deliberately withdrawn from the assimilation, such as a NOAA Gulfstream-IV flight is also shown. This need of an objective procedure to estimate the quality of an analysis is obvious and crucial in the scope of the re-analysis project of a field experiment such as FASTEX.

Acknowledgements

We are largely indebted to G. Jaubert and C. Piriou for making the FASTEX data quickly and easily available. We would also like to thank the French assimilation team and especially P. Caille for their kind support. The use of a high density network in the French variational assimilation scheme was first tested through the use of the FRONTS 92 dropsondes: we thank our British colleagues and more particularly S.A. Clough for providing this set of data. We also acknowledge Ph. Arbogast, J.P. Cammas, J.F. Geleyn, A. Joly and J. Pailleux for helpful discussion and comments.

8.6 References

Arbogast Ph. and A. Joly, 1998:
Precursor identification of a cyclogenesis.
Comptes Rendus de l'Académie des Sciences, **326**, 227–230.

Bergot T., 1999:
Adaptive observations during FASTEX: a systematic survey of upstream flights.
Quart. J. Roy. Meteor. Soc., *submitted*.

Bouttier, F., J. Derber and M. Fisher, 1997:
The 1997 revision of the J_b term in 3D/4D-Var.
ECMWF Tech. Memo., **238,** ECMWF Reading, 54 pp.

K.A. Browning, 1990:
Organization of clouds and precipitation in extratropical cyclones.
In *Extratropical cyclones: the Erik Palmén Memorial Volume*, pages 129–153. C.W. Newton and E.O. Holopainen, eds American Society.

K.A. Browning, S.P. Ballard, and C.S.A. Davitt, 1996:
High resolution analysis of frontal fracture.
Mon. Wea. Rev., **125**, 1212–1230.

K.A. Browning, S.A. Clough, C.S. Davitt, and N.M. Roberts, 1995:
Observations of the mesoscale sub-structure in the cold air of a developing frontal cyclone.
Quart. J. Roy. Meteor. Soc., **121**, 1229–1254.

J.P. Cammas, B. Pouponneau, G. Desroziers, and P. Santurette, 1999:
Initiation, trigerring and development phases of the FASTEX cyclone IOP 17: Synoptic and dynamic overview.
Quart. J. Roy. Meteor. Soc., *submitted*.

P. Courtier and J.-F. Geleyn, 1988:
A global numerical weather model with variable resolution: application to the shallow-water equations.
Mon. Wea. Rev., **114**, 1321–1346.

P. Courtier, C. Freydier, J.-F. Geleyn, F. Rabier, and M. Rochas, 1991:
The Arpege project at Météo-France.

In *Proceedings of the ECMWF Workshop on Numerical methods in atmospheric models*, pages 193–231, Reading.
9-13 September.

Courtier, P., J.-N. Thépaut and A. Hollingsworth, 1994:
A strategy for the operational implementation of 4D-Var, using an incremental approach.
Q. J. R. Meteorol. Soc., **120,** 1367–1387.

G. Desroziers and J. P. Lafore, 1993:
A coordinate transformation for objective frontal analysis.
Mon. Wea. Rev., **121**, 1531–1553.

Desroziers, G., V. Mathiot, F. Orain, and P. Bernardet, 1995:
Estimation locale des covariances d'erreurs de prévision d'un modèle spectral sur la sphère: Application au modèle à résolution variable ARPEGE.
Technical Report 34, CNRM/GMME, available from Météo-France.

G. Desroziers, B. Nechad, W. Sadiki, and J.-N. Thépaut.
Analyse variationnelle du réseau de dropsondes de l'expérience FRONTS 92: application du 3D-Var Arpège et discussion de l'erreur due à la formulation incrémentale de l'analyse à partir d'une maquette 1D-Var sur le cercle.
Technical Report 53, CNRM, 1997.

Desroziers, G., B. Pouponneau, J.N. Thépaut, M. Janisková, and F. Veersé, 1999:
Four dimensional variational analyses of FASTEX situations. part II: use of additional observations.
Quart. J. Roy. Meteor. Soc., **125**, *submitted.*

Gilbert, J.-Ch. and C Lemaréchal, 1989:
Some numerical experiments with variable storage quasi-Newton algorithms.
Mathematical Programming, **B 25,** 407–435.

Hardiker, V., 1997:
A Global Numerical Weather Prediction Model with Variable Resolution.
Mon. Wea. Rev., **125,** 59–73.

B.J. Hoskins, M.E. McIntyre, and A.W. Robertson, 1985.
On the use and significance of isentropic potential vorticity maps.
Quart. J. Roy. Meteor. Soc., **111**, 877–946.

Ide, K., P. Courtier, M. Ghil and A.C. Lorenc, 1997:
Unified Notation for Data Assimilation: Operational, Sequential and Variational.
J. Meteor. Soc. Japan, **75-1B,** 181–189.

Janisková, M., J.-N. Thépaut and J.-F. Geleyn, 1998:
Simplified and regular physical parametrizations for incremental four-dimensional variational assimilation.
Mon. Wea. Rev., *in press.*

M. Janisková, F. Veersé, J.-N. Thépaut, G. Desroziers, and B. Pouponneau, 1999:
Four dimensional variational analyses of FASTEX situations - Part I: Impact of a simplified physical package in the assimilating model.
Quart. J. Roy. Meteor. Soc., *submitted.*

G. Jaubert, C. Piriou, M.L. Scot, A. Petitpa, and J.A. Moore, 1999.
The FASTEX experiment Data Archive.
Quart. J. Roy. Meteor. Soc., *submitted.*

Joly, A., D.Jorgensen, M.A.Shapiro, A.Thorpe, P.Bessemoulin, K.A.Browning, J.P.Cammas, J.P.Chalon, S.A.Clough, K.A.Emanuel, L.Eymard, R.Gall, P.H.Hildebrand, R.H.Langland, Y.Lemaitre, P.Lynch, J.A.Moore, P.O.G.Persson, C.Snyder, R.M.Wakimoto, 1997:
The Fronts and Atlantic Storm-Track Experiment (FASTEX): Scientific Objectives and Experimental Design.
Bull. Amer. Meteor. Soc., **78**, (9), 1917–1940.

Joly, A., K.A. Browning, P. Bessemoulin, J.P. Cammas, G. Caniaux, J.P. Chalon, S.A. Clough, R. Dirks, K.A. Emanuel, L. Eymard, R. Gall, T.D. Hewson, P.H. Hildebrand, D. Jorgensen, F. Lalaurette, R.H. Langland, Y. Lemaitre, P. Mascart, J.A. Moore, P.O.G. Persson, F. Roux, M.A. Shapiro, C. Snyder, Z. Toth, and R.M. Wakimoto, 1999:
Overview of the field phase of the Fronts and Atlantic Storm-Track Experiment (FASTEX) project.
Quart. J. Roy. Meteor. Soc., **125**, *submitted.*

D. Keyser and M.A. Shapiro, 1986:
A review of the structure and dynamics of upper-level frontal zones.
Mon. Wea. Rev., **114**, 452–499.

R. Laprise, 1992:
The resolution of global spectral models.
BAMS, **73**, *(9)*, 1453–1454.

Laroche, S. and P. Gauthier, 1998:
A validation of the incremental variational data assimilation in a two-dimensional turbulent flow.
Tellus, *in press.*

Le Dimet, F.-X. and O Talagrand, 1986:
Variational algorithms for analysis and assimilation of meteorological observations: theoretical

aspects.
Tellus, **38 A,** 97–110.

Lynch, P., D. Giard and V. Ivanovici, 1997:
Improving the Efficiency of a Digital Filtering Scheme for Diabatic Initialization.
Mon. Wea. Rev., **125,** 1976–1982.

M.P. Moine and F. Roux.
Dynamic and thermodynamic structure of the mid-latitude cyclone observed on 19 february 1997 during FASTEX.
In *Proceedings of the Conference on Cloud Physics*, Washington, 1998.
17-21 August.

Naughton, M., P. Courtier and W. Bourke, 1996:
Representation errors in various grid and spectral truncations for a symmetric feature on a sphere.
Q. J. R. Meteorol. Soc., **122,** 253–265.

C. Pires, R. Vautard, and O. Talagrand, 1996:
On extending the limits of variational assimilation in nonlinear chaotic systems.
Tellus, **48A**, 96–121.

F. Schmidt, 1977:
Variable fine mesh in spectral global model.
Beitr. Phys. Atmos., **50**, 211–217.

M.A. Shapiro and J.T. Hastings, 1973:
Objective cross-section analyses by Hermite polynomial interpolation on isentropic surfaces.
J. Appl. Meteor., **12**, 753–762.

Simmons, A. and D. Burridge, 1981:
An energy and angular momentum conserving vertical finite difference scheme and hybrid vertical coordinates.
Mon. Wea. Rev., **109,** 758–766.

J.-N. Thépaut, P. Alary, P. Caille, V. Cassé, J.-F. Geleyn, P. Moll, J. Pailleux, J.-M. Piriou, D. Puech , and F. Taillefer.
The operational global data assimilation system at météo-france.
In *Proceedings of HIRLAM 4 Workshop on Variational Analysis in Limited Area Models*, pages 25–31, Toulouse, 1998.

J.-N. Thépaut, P. Courtier, G. Belaud, and G. Lemaître, 1996:
Dynamical structure functions in a four-dimensional variational assimilation: A case study.
Quart. J. Roy. Meteor. Soc., **122**, 535–561.

A.J. Thorpe and S.A. Clough, 1991:
Mesoscale dynamics of cold fronts: structures described by dropsoundings in FRONTS 87.
Quart. J. Roy. Meteor. Soc., **117**, 903–941.

Veersé, F. and J.-N. Thépaut, 1998:
Multiple-truncation incremental approach for four-dimensional variational data assimilation.
Q. J. R. Meteorol. Soc., **124,** 1889–1908.

G. Wahba, D.R. Johnson, F. Gao, and J. Gong, 1995:
Adaptative tuning of numerical weather prediction models: randomized GCV in three- and four-dimensional data assimilation.
Mon. Wea. Rev., **123**, 3358–3369.

G. Wahba and J. Wendelberger, 1980:
Some new mathematical methods for variational objective analysis using splines and cross validation.
Mon. Wea. Rev., **108**, 1122–1143.